Impact of right ventricular and pulmonary vascular characteristics on Impella hemodynamic support in biventricular heart failure: A simulation study.

松下, 裕貴

Journal of Cardiology 85 (2025) 100–107

Contents lists available at ScienceDirect

Journal of Cardiology

journal homepage: www.elsevier.com/locate/jjcc

Original Article

Impact of right ventricular and pulmonary vascular characteristics on Impella hemodynamic support in biventricular heart failure: A simulation study

Hiroki Matsushita (MD) [a], Keita Saku (MD, PhD) [a,*], Takuya Nishikawa (MD, PhD) [b], Takashi Unoki (MD) [c], Shohei Yokota (MD) [a], Kei Sato (MD) [a], Hidetaka Morita (MD, PhD) [a], Yuki Yoshida (BE) [a], Masafumi Fukumitsu (MD, PhD) [a], Kazunori Uemura (MD, PhD) [a,d], Toru Kawada (MD, PhD) [a], Atsushi Kikuchi (MD) [e], Ken Yamaura (MD, PhD) [f]

[a] Department of Cardiovascular Dynamics, National Cerebral and Cardiovascular Center Research Institute, Suita, Japan
[b] Department of Research Promotion and Management, National Cerebral and Cardiovascular Center Research Institute, Suita, Japan
[c] Department of Cardiology and Intensive Care Unit, Saiseikai Kumamoto Hospital, Kumamoto, Japan
[d] NTTR-NCVC Bio Digital Twin Center, National Cerebral and Cardiovascular Center Research Institute, Suita, Japan
[e] Department of Cardiology, Osaka General Medical Center, Suita, Japan
[f] Department of Anesthesiology and Critical Care Medicine, Graduate School of Medical Sciences, Kyushu University, Fukuoka, Japan

ARTICLE INFO

Article history:
Received 12 April 2024
Received in revised form 23 July 2024
Accepted 29 July 2024
Available online 2 August 2024

Keywords:
Simulation
Heart failure
Impella
Hemodynamics
Pulmonary vascular resistance

ABSTRACT

Background: Impella (Abiomed, Danvers, MA, USA) is a percutaneous ventricular assist device commonly used in cardiogenic shock, providing robust hemodynamic support, improving the systemic circulation, and relieving pulmonary congestion. Maintaining adequate left ventricular (LV) filling is essential for optimal hemodynamic support by Impella. This study aimed to investigate the impact of pulmonary vascular resistance (PVR) and right ventricular (RV) function on Impella-supported hemodynamics in severe biventricular failure using cardiovascular simulation.

Methods: We used Simulink® (Mathworks, Inc., Natick, MA, USA) for the simulation, incorporating pump performance of Impella CP determined using a mock circulatory loop. Both systemic and pulmonary circulation were modeled using a 5-element resistance–capacitance network. The four cardiac chambers were represented by time-varying elastance with unidirectional valves. In the scenario of severe LV dysfunction (LV end-systolic elastance set at a low level of 0.4 mmHg/mL), we compared the changes in right (RAP) and left atrial pressures (LAP), total systemic flow, and pressure–volume loop relationship at varying degrees of RV function, PVR, and Impella flow rate.

Results: The simulation results showed that under low PVR conditions, an increase in Impella flow rate slightly reduced RAP and LAP and increased total systemic flow, regardless of RV function. Under moderate RV dysfunction and high PVR conditions, an increase in Impella flow rate elevated RAP and excessively reduced LAP to induce LV suction, which limited the increase in total systemic flow.

Conclusions: PVR is the primary determinant of stable and effective Impella hemodynamic support in patients with severe biventricular failure.

Introduction

The incidence of heart failure increases as the population ages [1], with cardiogenic shock representing 2–5 % of acute heart failure cases, nearly half of which are fatal [2]. Impella (Abiomed, Danvers, MA, USA), a percutaneous left ventricular (LV) assist device (LVAD), is increasingly used in acute cardiac diseases, including ischemic heart disease and myocarditis. By reducing LV end-diastolic pressure and increasing total systemic flow, Impella effectively relieves lung congestion and improves systemic conditions during cardiogenic shock [3].

For optimal hemodynamic management using Impella, achieving sufficient LV filling through robust right ventricular (RV)–cardiac output (CO) is essential: Insufficient LV filling may result in excessive LV volume reduction by Impella, causing LV suction and diminished hemodynamic

* Corresponding author at: Department of Cardiovascular Dynamics, National Cerebral and Cardiovascular Center, Suita, 6-1 Kishibe-Shimmachi, Osaka 564-8565, Japan.
E-mail address: saku.keita@ncvc.go.jp (K. Saku).

https://doi.org/10.1016/j.jjcc.2024.07.008

support effects [4]. Based on the pressure-volume (PV) loop concept, the balance between RV function, preload, and afterload determines the RV–CO [5]. While Impella augments systemic flow and RV preload, it also reduces left atrial pressure (LAP), a component of RV afterload [6].

Clinical studies in patients with LVAD have demonstrated that RV function and pulmonary vascular resistance (PVR) are crucial elements in the pathogenesis of stable support [7,8]. However, considering the complexity and variability of RV function, PVR, and mechanical circulatory support (MCS) in clinical practice, it is challenging to clarify the relationship between these cardiovascular parameters and MCS operation based solely on clinical data. In this context, a comprehensive simulation study allows the manipulation of various parameters and the simultaneous evaluation of diverse hemodynamic impacts, enabling the visualization of the fundamental mechanism. Therefore, this integrated understanding of hemodynamic simulations plays a pivotal role in determining treatment strategies and optimizing MCS support for patients with biventricular failure (BVF).

This study aimed to determine the impact of PVR and RV function on Impella-supported hemodynamics in patients with severe BVF. We modeled the systemic and pulmonary circulation and pump characteristics of Impella and simulated hemodynamics using an electrical model. We evaluated changes in the right atrial pressure (RAP), LAP, and total systemic flow with variations in the Impella flow rate, RV function, and PVR.

Methods

Electrical model

We examined the impact of PVR and RV function on Impella-supported hemodynamics by in-silico analysis with a 5-element cardiovascular model (Fig. 1). The dynamic cardiovascular system was simulated using Simulink® (MathWorks, Natick, MA, USA). Both the systemic and pulmonary circulation were modeled using a 5-element resistance–capacitance network model. The four intracardiac valves were approximated as unidirectional valves and the flow rate was determined by the pressure gradient between the pre- and post-valve compartments and the valve orifice area based on Bernoulli's theorem [9]. In the four cardiac chambers, contractility and relaxation were represented by time-varying elastance [10] and stiffness was expressed by the end-diastolic pressure volume relationship [11]. Impella was designed to continuously withdraw blood from the LV and return it to the systemic artery using an axial pump. The characteristics of axial pumps can be explained using the pressure head-flow (H-Q) curve, where the flow is linked to the pressure gradient between the inlet and outlet of the catheter, as well as the pump rotation speed determined. Although the H-Q curve of Impella CP has been published previously, detailed numerical information was not provided. We evaluated the H-Q curve with mock circulation (Online Material, Online Fig. 1) and confirmed its consistency with the published characteristics. Thus, we used the pump characteristics obtained from the mock circulation in our simulation. When the Impella support level (P level) was set to a value between P1 and P9, the Impella flow rate was determined by the P level and the pressure gradient between the LV and the systemic artery, following the H-Q curve (Online Fig. 2).

Setting of parameters and outcomes

To simulate BVF without any MCS, we adjusted parameters as follows: LV end-systolic elastance (LV–E_{es}) was set at 0.4 mmHg/mL; RV–E_{es} was varied from almost zero to 0.4 mmHg/mL; heart rate was maintained at a constant 80 beats per minute, and systemic vascular resistance was set at 11.7 Wood units (WU), defined as the sum of the characteristic impedance (Zc) of systemic circulation, resistance of systemic artery, capillary vessels, and vein. Ventricular elastance was maintained throughout the cardiac cycle at a higher level than the end-diastolic pressure–volume relationship (EDPVR). Previous studies have reported normal values of 1.6 mmHg/mL for LV–E_{es} and 0.44 mmHg/mL for RV–

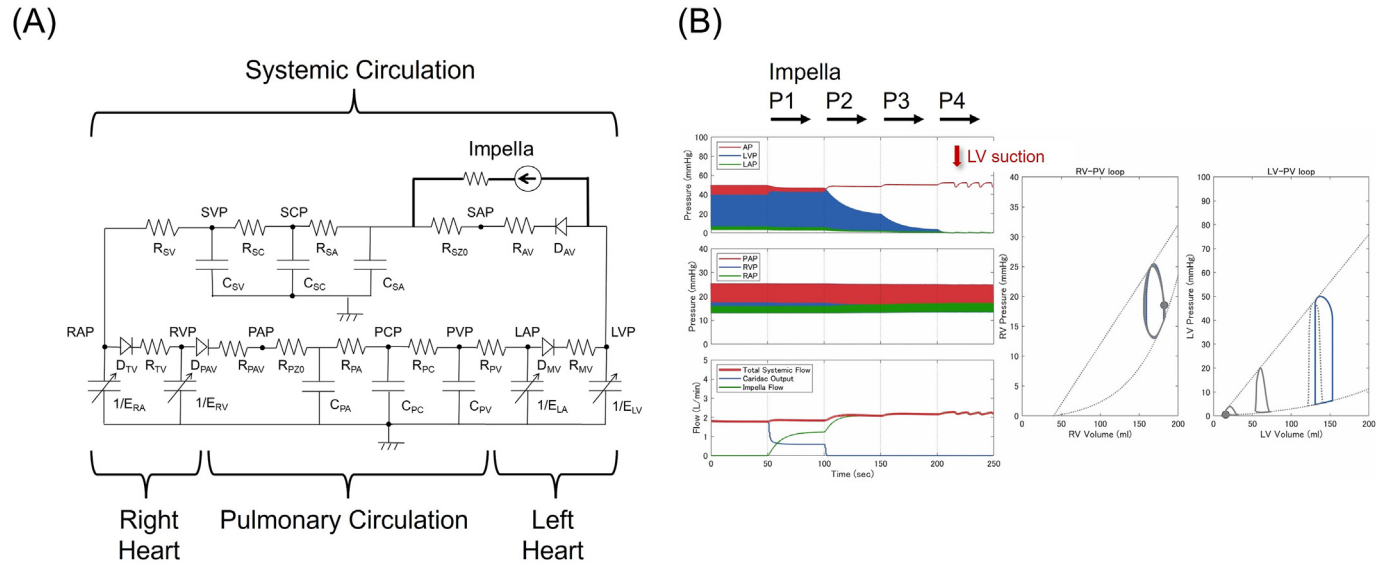

Fig. 1. Cardiovascular simulation model. (A) Circuit diagram of cardiovascular simulation model.
LAP, left atrial pressure; LVP, left ventricle pressure; SAP, systemic arterial pressure; SCP, systemic capillary pressure; SVP, systemic venous pressure; RAP, right atrial pressure; RVP, right ventricular pressure; PAP, pulmonary artery pressure; PCP, pulmonary capillary pressure; PVP, pulmonary venous pressure; E_{LA}, time-varying elastance of left atrium; D_{MV}, mitral valve; R_{MV}, resistance of mitral valve; E_{LV}, time-varying elastance of left ventricle; D_{AV}, aortic valve; R_{AV}, resistance of aortic valve; R_{SZ0}, characteristic impedance of systemic circulation; C_{SA}, compliance of systemic circulation; R_{SA}, resistance of systemic artery; C_{SC}, compliance of systemic capillary vessels; R_{SC}, resistance of systemic capillary vessels; C_{SV}, compliance of systemic vein; R_{SV}, resistance of systemic vein; E_{RA}, time-varying elastance of right atrium; D_{TV}, tricuspid valve; R_{TV}, resistance of tricuspid valve; E_{RV}, time-varying elastance of right ventricle; D_{PAV}, pulmonary artery valve; R_{PAV}, resistance of pulmonary artery valve; R_{PZ0}, characteristic impedance of pulmonary circulation; C_{PA}, compliance of pulmonary artery; R_{PA}, resistance of pulmonary artery; C_{PC}, compliance of pulmonary capillary vessels; R_{PC}, resistance of pulmonary capillary vessels; C_{PV}, compliance of pulmonary vein; R_{PV}, resistance of pulmonary vein.
(B) Representative plots from cardiovascular simulation. Our simulation captured complicated hemodynamic changes with Impella support and generated biventricular PV loops for each heartbeat.
AP, arterial pressure; LVP, left ventricular pressure; LAP, left atrial pressure; PAP, pulmonary artery pressure; RVP, right ventricular pressure; RAP, right atrial pressure; RV, right ventricle; LV, left ventricle; PV, pressure-volume.

E_{es}, although these values may vary depending on the species and method of measurement [12,13]. Each E_{es} in this study was set with reference to studies in models of cardiogenic shock caused by acute myocardial infarction or acute pulmonary artery thrombosis, that showed that contractility was reduced by 34–51 % from baseline [14,15]. We adjusted the stressed blood volume to maintain a mean artery pressure of approximately 60 mmHg in patients with BVF without Impella support.

PVR was defined as the sum of the Zc of pulmonary circulation, resistance of pulmonary artery, capillary vessels, and vein. To modify PVR, we adjusted pulmonary artery resistance and Zc, as reported in a previous study [16], whereas systemic and other physiological parameters were fixed based on data from healthy subjects (Online Table 2). PVR and pulmonary vascular compliance (PVC) exhibit an inverse relationship as pulmonary hypertension (PH) progresses, and the product of PVR and PVC (RC time) remains constant [17]. To validate the impact of PVR and PVC on Impella-supported hemodynamics, we tested two patterns of PVC setting: fixed PVC (Protocol 2, see below) and PVC altered according to the change in PVR to obtain a constant RC time (Protocol 3).

We constructed PV loops from the dynamic data obtained over time by conducting a simulation for each condition. We calculated the pressure–volume area (PVA) [18] by integrating the area enclosed by the end-systolic pressure–volume relationship (ESPVR), EDPVR, and the PV loop (Online Fig. 3). Additionally, we determined the stroke work (SW) [18] as the area within the PV loop for a single cardiac cycle. We compared the changes in RAP and LAP, total systemic flow, PVA, and SW under various degrees of RV function (RV–E_{es}: almost zero to 0.4 mmHg/mL), PVR (0.8 to 9.0 WU), and Impella flow rate. We also compared the RV– and LV–PV loops for each condition.

In clinical practice, excessive blood withdrawal by Impella can lead to a significant decrease in LV volume, resulting in “LV suction” [4]. In this study, LV suction was defined as LAP of below 0 mmHg. For clarity, figures do not show data points beyond this value (i.e. when LV suction occurs).

Protocols

Protocol 1: hemodynamic impact of varying RV–E_{es} and Impella flow rate

We examined the effect of Impella flow rate on hemodynamics with varying degrees of RV systolic function. RV–E_{es} was varied over a range of almost zero to 0.4 mmHg/mL. PVR was set at normal and high levels, whereas PVC was fixed at the normal level (PVR, 0.8 and 6.0; WU, PVC, 12 mmHg/mL).

Protocol 2: hemodynamic impact of varying PVR with fixed PVC and Impella flow rate

We investigated the impact of Impella flow rate on hemodynamics at varying levels of PVR. PVR was varied over a range of 0.8 to 9.0 WU. RV–E_{es} and PVC were fixed at 0.2 mmHg/mL and 12 mmHg/mL, respectively (Online Table 3).

Protocol 3: hemodynamic impact of PVR (constant RC time) and Impella flow rate

We investigated the impact of Impella flow rate on hemodynamics at varying levels of PVR. RV–E_{es} was set at 0.2 mmHg/mL, while PVR was varied over a range of 0.8 to 9.0 WU, and PVC was adjusted with change in PVR to maintain a constant RC time (Online Table 3).

Data analysis

The fixed-step size (fundamental sampling time) in this simulation was set at 0.2 ms, and we performed calculations for 550 s in each simulation. For the first 100 s, hemodynamic simulations were conducted without Impella support. The Impella flow rate was then increased gradually every 50 s, and stable hemodynamic values were extracted 2 s before the next alteration when the time series data reached a steady state (Online Fig. 4) [19].

Results

Protocol 1: impact of RV–E_{es} and Impella flow rate on hemodynamics

As shown in Fig. 2, a decrease in RV–E_{es} increased RAP and decreased LAP, CO, and total systemic flow with a low PVR (0.8 WU). An increase in the Impella flow rate determined by the H-Q curve resulted in an improvement in the total systemic flow with slight decreases in both RAP and LAP, regardless of RV–E_{es}. In the PV loop analysis, an increase in the Impella support level from P2 to P6 resulted in a slight leftward

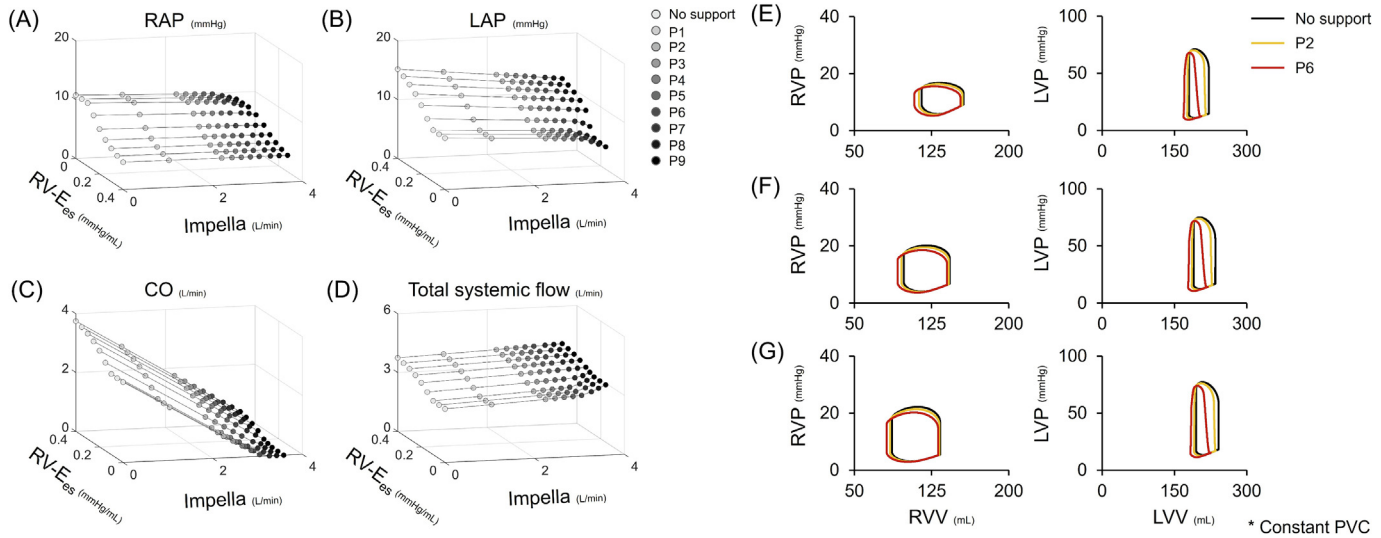

Fig. 2. Impact of RV–E_{es} and Impella flow rate on hemodynamics in low PVR conditions. Changes in (A) RAP, (B) LAP, (C) CO, (D) total systemic flow, and three conditions of right and left ventricular PV loops (E) 0.2 mmHg/mL, (F) 0.3 mmHg/mL, and (G) 0.4 mmHg/mL are shown in low PVR conditions (0.8 WU). Each simulation from (A) to (D) consisted of a series of 10 plots (without support and with Impella support, varying settings from levels P1 to P9). A decrease in RV–E_{es} increased RAP and decreased LAP, CO, and total systemic flow. An increase in the Impella flow rate improved the total systemic flow, with slight decreases in both RAP and LAP, regardless of RV–E_{es}. From (E) to (G), the colored lines representing different Impella support levels are black, baseline (without support); yellow, P2; and red, P6. An increase in Impella support level from baseline to P6 resulted in a slight leftward shift in the RV–PV loop. The same trend was observed for RV–E_{es} from 0.2 to 0.4 mmHg/mL.
RV–E_{es}, right ventricular end-systolic elastance; PV loops, pressure-volume loops; PVR, pulmonary vascular resistance; WU, Wood units; RAP, right atrial pressure; LAP, left atrial pressure; CO, cardiac output; RVP, right ventricular pressure; RVV, right ventricular volume; LVP, left ventricular pressure; LVV, left ventricular volume.

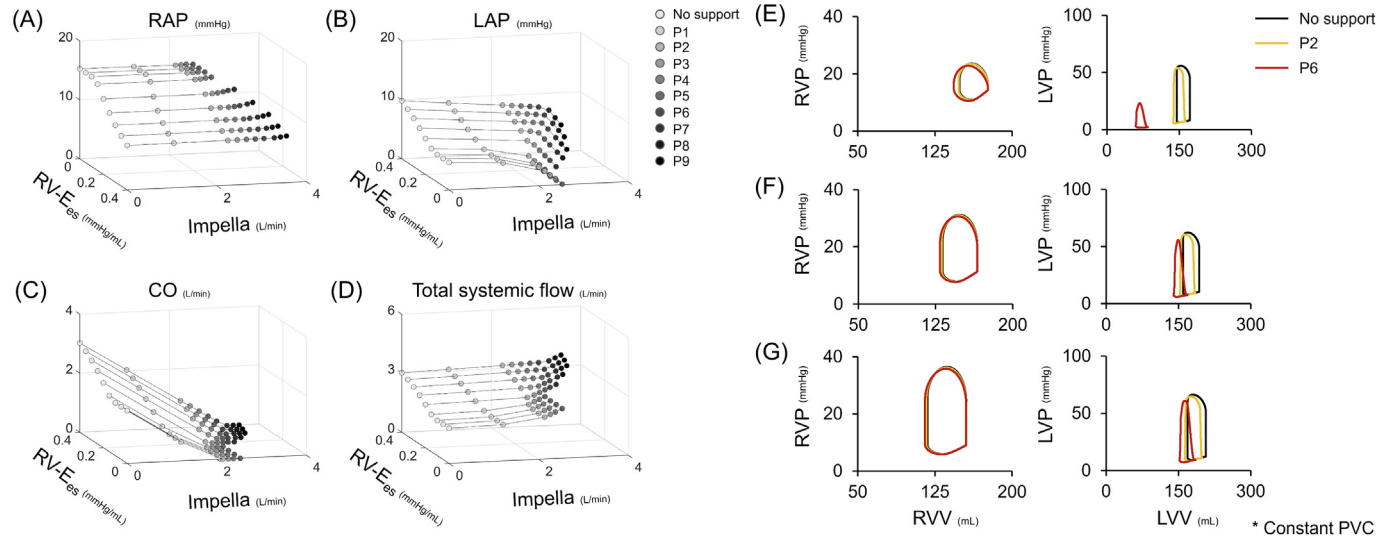

Fig. 3. Impact of RV–E_{es} and Impella flow rate on hemodynamics in high PVR conditions. Changes in (A) RAP, (B) LAP, (C) CO, (D) total systemic flow, and three conditions of right and left ventricular PV loops (E) 0.2 mmHg/mL, (F) 0.3 mmHg/mL, and (G) 0.4 mmHg/mL are shown in high PVR conditions (6.0 WU). An increase in the Impella flow rate reduced LAP regardless of PVR; however, when RV–E_{es} was <0.25 mmHg/mL, an increase in the Impella flow rate reduced LAP excessively and induced LV suction. An increase in the Impella support level from baseline to P6 resulted in a slight leftward shift in the RV–PV loop. The same trend was observed at RV–E_{es} from 0.2 to 0.4 mmHg/mL, similar to those in low PVR conditions. This was accompanied by a significant increase in RV end-systolic pressure.
RV–E_{es}, right ventricular end-systolic elastance; PV loops, pressure-volume loops; PVR, pulmonary vascular resistance; WU, Wood units; RAP, right atrial pressure; LAP, left atrial pressure; CO, cardiac output; RVP, right ventricular pressure; RVV, right ventricular volume; LVP, left ventricular pressure; LVV, left ventricular volume.

shift of the RV–PV loop. The same trend was observed at three RV–E_{es} levels between 0.2 and 0.4 mmHg/mL. Meanwhile, an increase in the Impella flow also shifted the LV–PV loop left downward and reduced both LV–PVA and LV–SW (Online Table 4).

Under high PVR conditions (6.0 WU), as shown in Fig. 3, a decrease in RV function indicated a similar trend in hemodynamic changes to those observed under low PVR conditions (Fig. 2). However, an increase in the Impella flow rate did not change RAP in low RV–E_{es} but significantly increased RAP in relatively preserved RV function. An increase in the Impella flow rate reduced LAP regardless of PVR; however, when RV–E_{es} was <0.25 mmHg/mL, an increase in the Impella flow rate reduced LAP excessively and induced LV suction. LV suction limited high Impella support levels, resulting in a total systemic flow below 3.2 L/min. In the PV loop analysis, an increase in the Impella support level from P2 to P6 resulted in a slight leftward shift in the RV–PV loop and a significant leftward shift in the LV–PV loop. The expansion of the RV–PV loop to the left and LV–PV loop to the right were observed because of the increase in RV–E_{es} from 0.2 to 0.4 mmHg/mL. This was accompanied by a significant increase in RV end-systolic pressure (RVESP) and RV–PVA (Online Table 5).

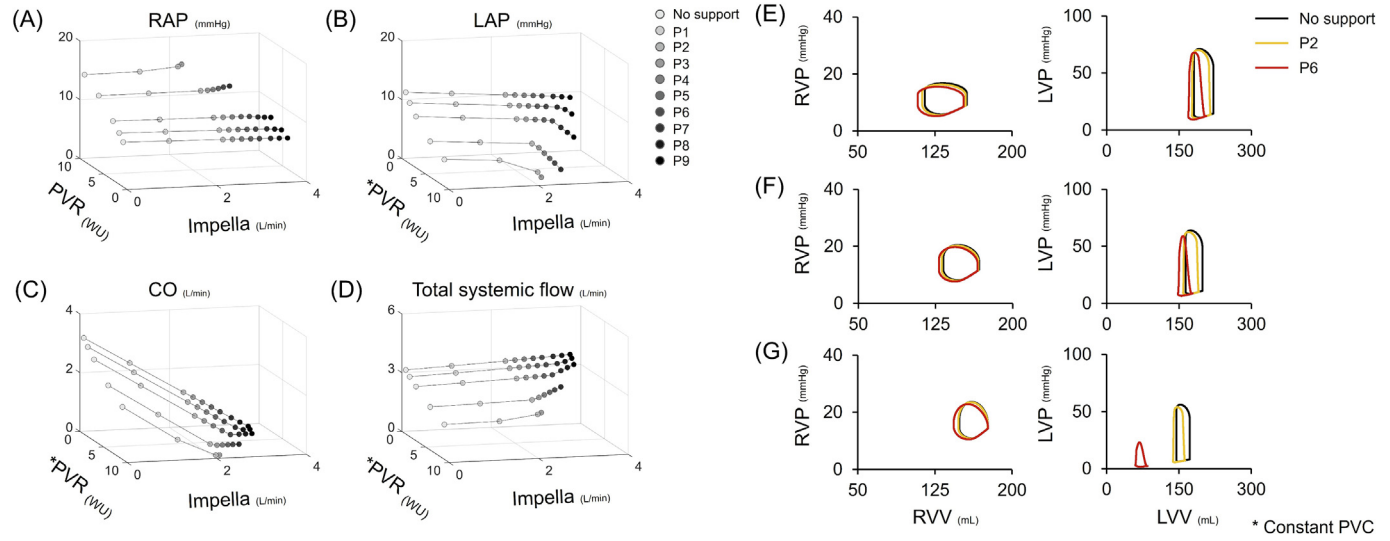

Fig. 4. Impact of PVR with fixed PVC and Impella flow rate on hemodynamics. Changes in (A) RAP, (B) LAP, (C) CO, (D) total systemic flow, and three conditions of right and left ventricular PV loops (E) 0.8 WU, (F) 3.0 WU, and (G) 6.0 WU are shown. Asterisk (*) indicates that the corresponding axis has been inverted for clarity or for highlighting specific relationships. An increase in PVR elevated the RAP while reducing LAP, CO, and total systemic flow. An increase in Impella flow rate decreased RAP at low PVR but significantly increased RAP at higher PVR conditions. Increased Impella flow rates reduced LAP regardless of PVR; however, under extremely high PVR conditions, an increase in Impella flow rate reduced LAP excessively and induced LV suction. LV suction prevented the plotting of points over Impella level P7 (2.3 L/min of total systemic flow). An increase in Impella support level from baseline to P6 shifted the RV–PV loop slightly to the left and downward in the low-PVR condition. Increasing the Impella flow rate slightly widened the RV–PV loop under high-PVR conditions.
PVR, pulmonary vascular resistance; WU, Wood units; PVC, pulmonary vascular compliance; PV loops, pressure-volume loops; RVP, right ventricular pressure; RVV, right ventricular volume; LVP, left ventricular pressure; LVV, left ventricular volume.

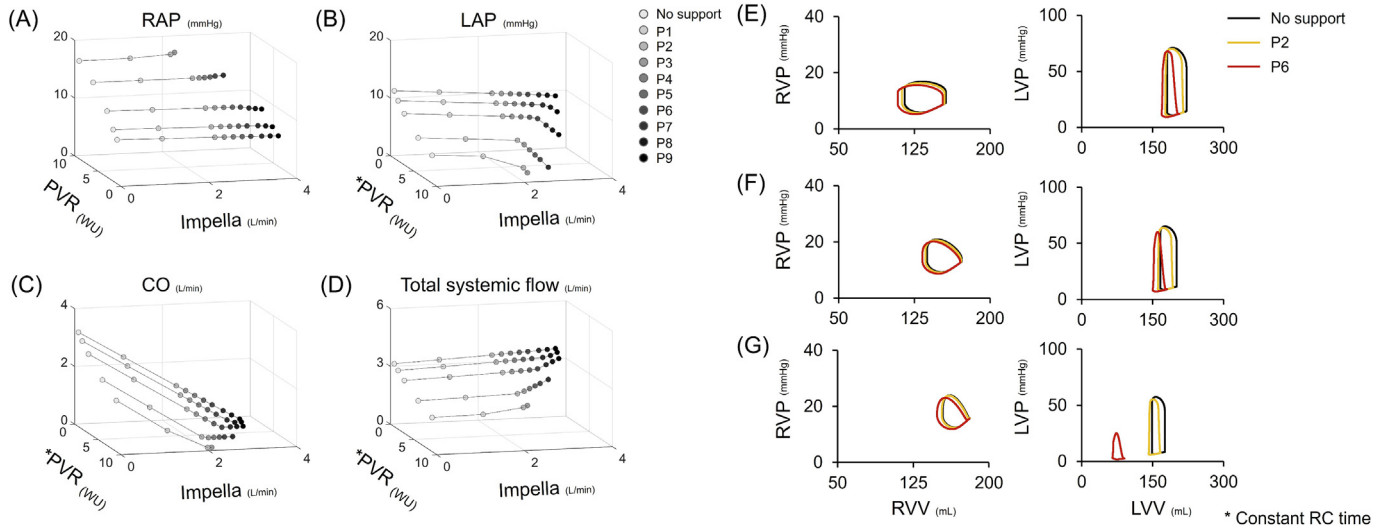

Fig. 5. Impact of PVR (constant RC time) and Impella flow rate on hemodynamics. Changes in (A) RAP, (B) LAP, (C) CO, (D) total systemic flow, and three conditions of right and left ventricular PV loops (E) 0.8 WU, (F) 3.0 WU, and (G) 6.0 WU are shown. An increase in PVR resulted in a decrease in PVC to maintain a constant RC time. Although a reduction in PVC was accompanied by an increase in PVR elevated RAP, the trend of hemodynamic changes with increases in Impella flow rate was the same as that in Protocol 2 under all PVR conditions tested. The RV–PV loop showed a slightly triangular shape at a high PVR, but the changes with increasing Impella support level were the same as those in protocol 2. Impella also shifted the left and downward LV-PV loops, as in Protocol 2.
PVR, pulmonary vascular resistance; PVC, pulmonary vascular compliance; WU, Wood units; RC time, product of PVR and PVC; PV loops, pressure-volume loops; RAP, right atrial pressure; LAP, left atrial pressure; CO, cardiac output; RVP, right ventricular pressure; RVV, right ventricular volume; LVP, left ventricular pressure; LVV, left ventricular volume.

Protocol 2: impact of PVR with fixed PVC and Impella flow rate on hemodynamics

An increase in PVR elevated RAP, while reducing LAP, CO, and total systemic flow (Fig. 4). An increase in the Impella flow rate decreased RAP under low PVR conditions but significantly increased RAP under high PVR conditions. An increase in the Impella flow rate reduced LAP regardless of PVR; however, under extremely high PVR conditions, an increase in the Impella flow rate reduced LAP excessively and induced LV suction. LV suction limited Impella support above the P7 level (2.3 L/min of total systemic flow). In the PV loop analysis, an increase in the Impella flow rate shifted the RV–PV loop slightly downward under the low PVR condition. Increasing the Impella flow rate widened the RV–PV loop leftward in the high PVR condition. An increase in the Impella flow rate also shifted the LV–PV loop left downward and reduced both LV–PVA and LV–SW (Online Table 6).

Protocol 3: impact of PVR (constant RC time) and Impella flow rate on hemodynamics

In this simulation, an increase in PVR resulted in a decrease in PVC to maintain a constant RC time. Although a reduction in PVC accompanied by an increase in PVR elevated RAP, the trend of hemodynamic changes with an increase in the Impella flow rate was the same as that in Protocol 2 under all PVR conditions (Fig. 5). In the PV loop analysis, the RV–PV loop showed a slightly triangular shape at a high PVR; however, the changes with increasing Impella flow rate were the same as those in Protocol 2. An increase in the Impella flow rate also shifted the LV–PV loop left downward and reduced both the LV–PVA and LV–SW (Online Table 7), as in Protocol 2.

Discussion

In this study, we used cardiovascular simulation to investigate the effect of pulmonary circulation on Impella-supported hemodynamics in patients with severe BVF. The major findings of our study were as follows: (1) At low PVR, even when RV– E_{es} was extremely low, Impella was able to maintain the circulation; (2) at high PVR (with fixed PVC), Impella-supported circulation became unstable owing to reduced RV–CO and LV filling; and (3) the same findings were obtained when PVC was varied to maintain a constant RC time.

Impact of right ventricular and pulmonary vascular characteristics on Impella-supported hemodynamics and RV workload in BVF

This study demonstrated the importance of PVR in hemodynamics, supported by Impella. Under low PVR conditions, Impella effectively maintained the simulated pulmonary circulation, even when the RV–E_{es} was notably low (Fig. 2). This is analogous to a previous clinical report demonstrating successful LVAD placement in a patient with Fontan circulation who had no RV function and a low PVR [20]. Under high PVR conditions (6.0 WU) at preserved RV function, Impella maintained hemodynamics. Meanwhile, an increase in the Impella support levels resulted in excessive LAP reduction and LV suction at impaired RV function (≤ 0.25 mmHg/mL) with high PVR. In addition, lower RV function induced LV suction at lower Impella support levels. Thus, a balance between PVR and RV function determined whether Impella can provide effective hemodynamic support under high PVR conditions. In LVAD-supported hemodynamics, RV function and PVR are important factors for stability [7,8]. However, to the best of our knowledge, there have been no integrated analyses of the relationships between RV function, PVR, and LVAD flow. Furthermore, this understanding may be more important in Impella-supported hemodynamics, where flow is more limited than that in LVAD. Our simulations showed that the sensitivity of RV function to stable Impella support may differ between low- and high-PVR conditions, indicating the importance of PVR regulation in Impella-supported hemodynamics.

As shown in Fig. 2, we visualized the biventricular workload under Impella support using simulations of various degrees of RV failure. When PVR was low, increases in the Impella support widened and shifted the RV-PV loop to the left. This indicates a significant decrease in RV afterload and an increase in RV–stroke volume (SV) despite an increase in venous return to the RV. As LAP may contribute to RV afterload significantly more than PVR under low PVR conditions, LV unloading by Impella markedly decreases RV afterload, resulting in increased RV–CO. Meanwhile, when PVR was extremely high, Impella support increased RAP, indicating exacerbated RV failure (Figs. 4 and 5). In addition, Impella support widened the RV–PV loop without changing the end-systolic

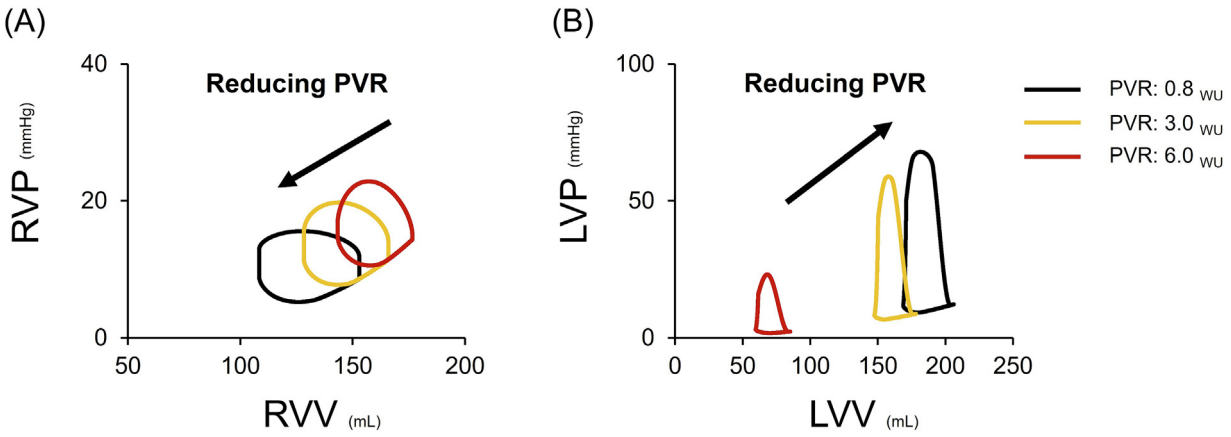

Fig. 6. Impact of the reduction in PVR with fixed PVC at Impella support level P6 on right and left ventricular PV loops. PVR conditions are represented by various line colors: black, 0.8; yellow, 3.0; red, 6.0 WU. RV function was severely impaired (0.2 mmHg/mL). Black arrows indicate the directional change in both (A) RV-PV and (B) LV–PV loops following a decrease in PVR. Severe RV systolic dysfunction resulted in the relative low RVP despite the increase of PVR. PVR reduction shifted the RV–PV loops left and downward, indicating a decrease in RV afterload and an increase in SV. Meanwhile, a reduction in PVR shifted the LV–PV loop right and upward, indicating an increase in LV filling.
PVR, pulmonary vascular resistance; PVC, pulmonary vascular compliance; WU, Wood units; RV–E_{es}, right ventricular end-systolic elastance; PV loops, pressure-volume loops; RVP, right ventricular pressure; RVV, right ventricular volume; LVP, left ventricular pressure; LVV, left ventricular volume; SV, stroke volume.

pressure, indicating an increase in both RV preload and RV–SV and a slight decrease in RV afterload (Online Fig. 5). Our simulation clarified how PVR affects Impella-supported hemodynamics and RV workload in patients with BVF, highlighting the importance of PVR in clinical practice.

In clinical practice, inotropes are commonly used to maintain RVCO after LVAD implantation [21]. As shown in Fig. 3, even in high PVR conditions (PVR: 6.0 WU), the improvement in RV function prevented LV suction, which occurred in low RV function (RV–E_{es} ≤ 0.25 mmHg/mL). In PV loop analysis, RV end-systolic pressure and RV–PVA were significantly elevated due to the increase in RV function (Fig. 7). Thus, an improvement in RV function may contribute to adequate LV filling and stable Impella support. However, it may also result in an increased risk of pulmonary bleeding due to elevated pulmonary artery pressure [22] and myocardial oxygen supply and demand imbalance under high PVR conditions.

Cardiovascular simulation can provide an understanding of circulatory dynamics beyond clinical experience by varying a specific parameter. On the other hand, several investigations in patients with PH have suggested that PVR may increase following a decrease in PVC [23,24]. Therefore, we performed an analysis in which pulmonary artery compliance was adjusted to maintain a constant RC time (Protocol 3), as shown in Fig. 5. Compared with the simulation with PVC fixed (Protocol 2, Fig. 4), a decrease in PVC accompanied by an increase in PVR elevated RAP and altered the shape of the RV–PV loop. Maughan et al. [25] reported that changes in arterial compliance in the isolated LV resulted in marked changes in the shape of the PV loop but did not significantly affect LV–SV, or consequently, E_a. Saouti et al. reported that pulsatile afterload due to a decrease in PVC in pulmonary circulation did not change with the progression of PH [26]. Our simulations revealed consistent hemodynamic changes due to alterations in the Impella flow rate in both the fixed and adjusted PVC scenarios, indicating that PVC had little influence on the efficiency of Impella support in clinical settings.

PVR modulation in clinical practice

Our simulations demonstrated that PVR is a critical parameter for maintaining effective Impella support in BVF. Inhaled nitric oxide (iNO) is a pulmonary vasodilator that selectively reduces PVR without significantly altering systemic hemodynamics [27]. Several studies have reported the use of iNO in patients with LVAD or Impella support [28,29], and iNO has become the standard of care for RV failure after LVAD implantation in many institutions [30]. Fig. 6 illustrates the impact of reducing PVR at level P6 of Impella support on both the RV and LV-PV loops extracted from Fig. 4. The reduction in PVR results in a decrease in RV afterload and an increase in RV–SV and LV filling, indicating effective

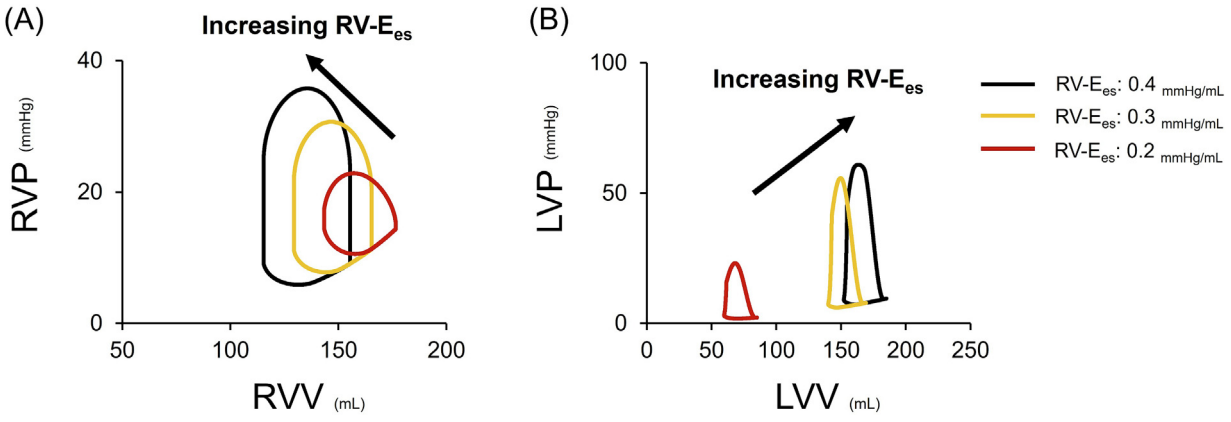

Fig. 7. Impact of the increase in RV–E_{es} at Impella support level P6 on right and left ventricular PV loops. RV functions are represented by colored lines: black, 0.4 mmHg/mL; yellow, 0.3 mmHg/mL; red, 0.2 mmHg/mL. PVR was set to a high level (6.0 WU). Black arrows indicate the directional change in both (A) RV-PV and (B) LV–PV loops following an increase in RV–E_{es}. Improvement in RV function shifted the RV–PV loops left and upward, indicating an increase in RV afterload and SV. An increase in RV–E_{es} shifts the LV–PV loop right and upward, indicating an increase in LV filling. Meanwhile, changes in the LV-PV loops with an increase in RV function were the same as those with a reduction in PVR.
PVR, pulmonary vascular resistance; PVC, pulmonary vascular compliance; WU, Wood units; RV–E_{es}, right ventricular end-systolic elastance; PV loops, pressure-volume loops; RVP, right ventricular pressure; RVV, right ventricular volume; LVP, left ventricular pressure; LVV, left ventricular volume; SV, stroke volume.

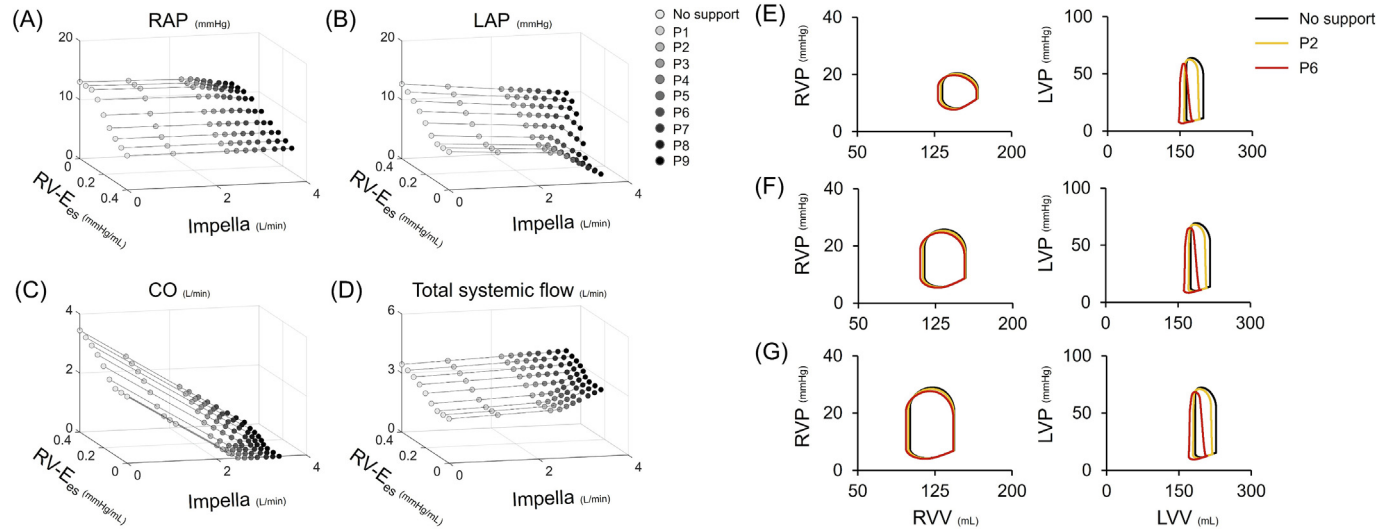

Fig. 8. Impact of RV–E_{es} and Impella flow rate on hemodynamics in upper normal levels of PVR conditions. Changes in (A) RAP, (B) LAP, (C) CO, (D) total systemic flow, and three conditions of right and left ventricular PV loops (E) 0.2 mmHg/mL, (F) 0.3 mmHg/mL, and (G) 0.4 mmHg/mL are shown in upper normal levels of PVR conditions (3.0 WU). The same trend was observed for each RV–E_{es} as in the low PVR conditions (0.8 WU).
RV–E_{es}, right ventricular end-systolic elastance; PV loops, pressure-volume loops; PVR, pulmonary vascular resistance; WU, Wood units; RAP, right atrial pressure; LAP, left atrial pressure; CO, cardiac output; RVP, right ventricular pressure; RVV, right ventricular volume; LVP, left ventricular pressure; LVV, left ventricular volume.

prevention of LV suction. Hence, our simulation provides a comprehensive explanation of the hemodynamics underlying the use of iNO for effective Impella support.

It would be ideal to know whether Impella can provide sufficient and stable support for each patient's PVR cut-off. However, the threshold at which PVR Impella alone provides sufficient hemodynamic support remains unknown. In a retrospective study by Cedars et al., the preoperative PVR in Fontan patients implanted with LVAD was 2.9 WU per m^2 [20], while Nitta et al. reported that >4.5 WU of PVR was a significant predictor for RV assist device requirement in LVAD patients [31]. Our simulation demonstrated that Impella was able to maintain stable hemodynamics at 3.0 WU of PVR regardless of RV function (Fig. 8). However, at 6.0 WU of PVR, a high Impella support rate induced LV suction below 0.25 mmHg/mL of RV function. Furthermore, lower RV function induced LV suction at a lower level of Impella support (Fig. 3). The range of cut-off values from the theoretical analysis and clinical studies showed remarkable similarity. Future patient-specific parameterization and further studies are required to determine whether the Impella device alone can provide adequate and stable hemodynamic support for BVF.

Limitations

This study had several limitations, primarily intrinsic to cardiovascular mathematical modeling. First, the simulation did not consider the variability in cardiovascular parameters, interventricular interactions, or respiration. In patients, various parameters, such as LV contractility, heart rate, vascular compliance, and resistance, can change owing to autonomic nerve activity through baroreceptors or cardiopulmonary reflexes [32]. Interventricular interactions through the ventricular septum have significant limitations. These interactions with increased LVAD flow have been reported to improve the RV–SV and compliance without compromising RV contraction [33]. Because our current simulations did not include the effects of interventricular interactions for simplicity, the potential improvement in RV compliance with increased Impella flow may result in greater RV output and LV filling, thus ensuring stable Impella support. In addition, anatomical changes in valve structure, such as mitral and tricuspid regurgitation with heart failure, were not considered in the simulation [34,35].

Second, this simulation may not accurately represent the behavior of Impella in the body. Because mock circulation inherently differs from the circulation in vivo and uses extracellular fluid instead of blood, the results obtained from the H-Q curve may not be directly applicable to clinical situations. In addition, the insertion of the Impella catheter may affect aortic valve regurgitation [36]. Although aortic valve regurgitation potentially reduces systemic flow during Impella support, it may also contribute to LV filling and reduce the risk of LV suction.

Third, interpretations derived from our simulation may not be applicable to every patient in the same situation. In this study, all cardiovascular parameters except RV function, PVR, and PVC were fixed. Our comprehensive analysis represents phenomena that may occur in specific situations; therefore, some patients may not benefit from these results. We previously reported the patient-specific simulation by using the same model [37]. In the next step, we plan to incorporate automated and patient-specific parameterization, which can help clinicians estimate individual hemodynamic changes and provide patient-tailored Impella therapy.

Conclusions

In cardiovascular simulation, PVR is the major determinant for achieving stable and effective Impella hemodynamic support in severe BVF. This study suggests that achieving a low PVR in severe BVF can effectively reduce RV afterload indirectly through the stable decrease of LAP with Impella.

Funding

This research was supported by grants from Grant-in-Aid for Scientific Research (JSPS KAKENHI 22K08222), the Japan Agency for Medical Research and Development (23hk0102085h0002, 23uk1024007h0001), the Ministry of Internal Affairs and Communications (SCOPE: JP225006004), the Intramural Research Fund for Cardiovascular Diseases of National Cerebral and Cardiovascular Center (21-2-7, 21-2-9), Japan Science and Technology Agency (JPMJPF2018), Abiomed Japan K.K., and NTT-Research, Inc.. The authors confirm that these parties did not influence the study design, content of the article, or selection of this journal.

Declaration of competing interest

Matsushita H, Nishikawa T, Unoki T, Yokota S, Sato K, Morita H, Yoshida Y, Fukumitsu M, Nishiura A, Uemura K, Kawada T, Kikuchi A,

and Yamaura K, declare no conflicts of interest. Saku K received research funding from Abiomed Japan K.K., NTT Research, Inc., Asahi Kasei ZOLL Medical Corporation, Neuroceuticals Inc., and Zeon Medical Inc. and honoraria from Abiomed Japan K.K., Mallinckrodt Pharma K.K., and Ono Pharmaceutical Co., Ltd.

Acknowledgments

We thank the Department of Cardiovascular Dynamics and National Cerebral and Cardiovascular Center staff. We would also like to sincerely thank MathWorks, Inc., for their invaluable support and contribution to this research. We would like to thank Teresa Nakatani and Editage (www.editage.jp) for English language editing.

Appendix A. Supplementary data

Supplementary data to this article can be found online at https://doi.org/10.1016/j.jjcc.2024.07.008.

References

[1] Murphy SP, Ibrahim NE, Januzzi Jr JL. Heart failure with reduced ejection fraction: a review. JAMA 2020;324:488–504.
[2] Chioncel O, Parissis J, Mebazaa A, Thiele H, Desch S, Bauersachs J, et al. Epidemiology, pathophysiology and contemporary management of cardiogenic shock - a position statement from the heart failure Association of the European Society of cardiology. Eur J Heart Fail 2020;22:1315–41.
[3] Burkhoff D, Sayer G, Doshi D, Uriel N. Hemodynamics of mechanical circulatory support. J Am Coll Cardiol 2015;66:2663–74.
[4] Møller JE, Hassager C, Bonello L, Delmas C, Pappalardo F. Pump flow setting and assessment of unloading in clinical practice. Eur Heart J Suppl 2021;23:A23–6.
[5] Uemura K, Kawada T, Kamiya A, Aiba T, Hidaka I, Sunagawa K, et al. Prediction of circulatory equilibrium in response to changes in stressed blood volume. Am J Physiol Heart Circ Physiol 2005;289:H301–7.
[6] Brener MI, Masoumi A, Ng VG, Tello K, Bastos MB, Cornwell 3rd WK, et al. Invasive right ventricular pressure-volume analysis: basic principles, clinical applications, and practical recommendations. Circ Heart Fail 2022;15:e009101.
[7] Sciaccaluga C, Procopio MC, Potena L, Masetti M, Bernazzali S, Maccherini M, et al. Right ventricular dysfunction in left ventricular assist device candidates: is it time to change our prospective? Heart Fail Rev 2024;29:559–69.
[8] Drakos SG, Janicki L, Horne BD, Kfoury AG, Reid BB, Clayson S, et al. Risk factors predictive of right ventricular failure after left ventricular assist device implantation. Am J Cardiol 2010;105:1030–5.
[9] Abbas AE, Mando R, Hanzel G, Goldstein J, Shannon F, Pibarot P. Hemodynamic principles of prosthetic aortic valve evaluation in the transcatheter aortic valve replacement era. Echocardiography 2020;37:738–57.
[10] Suga H, Sagawa K, Shoukas AA. Load independence of the instantaneous pressure-volume ratio of the canine left ventricle and effects of epinephrine and heart rate on the ratio. Circ Res 1973;32:314–22.
[11] Mirsky I. Assessment of passive elastic stiffness of cardiac muscle: mathematical concepts, physiologic and clinical considerations, directions of future research. Prog Cardiovasc Dis 1976;18:277–308.
[12] Baicu CF, Zile MR, Aurigemma GP, Gaasch WH. Left ventricular systolic performance, function, and contractility in patients with diastolic heart failure. Circulation 2005;111:2306–12.
[13] McCabe C, White PA, Hoole SP, Axell RG, Priest AN, Gopalan D, et al. Right ventricular dysfunction in chronic thromboembolic obstruction of the pulmonary artery: a pressure-volume study using the conductance catheter. J Appl Physiol 2014;116:355–63.
[14] Rienzo M, Imbault J, El Boustani Y, Beurton A, Carlos Sampedrano C, Pasdois P, et al. A total closed chest sheep model of cardiogenic shock by percutaneous intracoronary ethanol injection. Sci Rep 2020;10:12417.
[15] Kerbaul F, By Y, Gariboldi V, Mekkaoui C, Fesler P, Collart F, et al. Acute pulmonary embolism decreases adenosine plasma levels in anesthetized pigs. ISRN Cardiol 2011;2011:750301.
[16] Hungerford SL, Kearney K, Song N, Bart N, Kotlyar E, Lau E, et al. Prognostic role of pulmonary impedance estimation to predict right ventricular dysfunction in pulmonary hypertension. ESC Heart Fail 2023;10:1811–21.
[17] Lankhaar JW, Westerhof N, Faes TJ, Marques KM, Marcus JT, Postmus PE, et al. Quantification of right ventricular afterload in patients with and without pulmonary hypertension. Am J Physiol Heart Circ Physiol 2006;291:H1731–7.
[18] Suga H. Ventricular energetics. Physiol Rev 1990;70:247–77.
[19] Jones E, Randall EB, Hummel SL, Cameron DM, Beard DA, Carlson BE. Phenotyping heart failure using model-based analysis and physiology-informed machine learning. J Physiol 2021;599:4991–5013.
[20] Cedars A, Kutty S, Danford D, Schumacher K, ACTION Learning Network Investigators, Auerbach SR, et al. Systemic ventricular assist device support in Fontan patients: a report by ACTION. J Heart Lung Transplant 2021;40:368–76.
[21] Lampert BC, Teuteberg JJ. Right ventricular failure after left ventricular assist devices. J Heart Lung Transplant 2015;34:1123–30.
[22] Cantu J, Wang D, Safdar Z. Clinical implications of haemoptysis in patients with pulmonary arterial hypertension. Int J Clin Pract Suppl 2012;177:5–12.
[23] Mahapatra S, Nishimura RA, Sorajja P, Cha S, McGoon MD. Relationship of pulmonary arterial capacitance and mortality in idiopathic pulmonary arterialhypertension. J Am Coll Cardiol 2006;47:799–803.
[24] Sanz J, Kariisa M, Dellegrottaglie S, Prat-Gonzalez S, Garcia MJ, Fuster V, et al. Evaluation of pulmonary artery stiffness in pulmonary hypertension with cardiac magnetic resonance. JACC Cardiovasc Imaging 2009;2:286–95.
[25] Maughan WL, Sunagawa K, Burkhoff D, Sagawa K. Effect of arterial impedance changes on the end-systolic pressure-volume relation. Circ Res 1984;54:595–602.
[26] Saouti N, Westerhof N, Helderman F, Marcus JT, Boonstra A, Postmus PE, et al. Right ventricular oscillatory power is a constant fraction of total power irrespective of pulmonary artery pressure. Am J Respir Crit Care Med 2010;182:1315–20.
[27] Rossetti M, Guénard H, Gabinski C. Effects of nitric oxide inhalation on pulmonary serial vascular resistances in ARDS. Am J Respir Crit Care Med 1996;154:1375–81.
[28] Lovich MA, Pezone MJ, Wakim MG, Denton RJ, Maslov MY, Murray MR, et al. Inhaled nitric oxide augments left ventricular assist device capacity by ameliorating secondary right ventricular failure. ASAIO J 2015;61:379–85.
[29] Fujita K, Ueno M, Yasuda M, Mizutani K, Miyoshi T, Nakazawa G. Haemodynamic effects of inhaled nitric oxide in acute myocardial infarction complicated by right heart failure under ECPELLA support: case report. Eur Heart J Case Rep 2023;7:ytad369.
[30] Benedetto M, Romano R, Baca G, Sarridou D, Fischer A, Simon A, et al. Inhaled nitric oxide in cardiac surgery: evidence or tradition? Nitric Oxide 2015;49:67–79.
[31] Nitta D, Kinugawa K, Imamura T, Amiya E, Hatano M, Kinoshita O, et al. A useful scoring system for predicting right ventricular assist device requirement among patients with a paracorporeal left ventricular assist device. Int Heart J 2018;59:983–90.
[32] Triposkiadis F, Karayannis G, Giamouzis G, Skoularigis J, LouridasJ.Butler J. The sympathetic nervous system in heart failure physiology, pathophysiology, and clinical implications. J Am Coll Cardiol 2009;54:1747–62.
[33] Brener MI, Kanwar MK, Lander MM, Hamid NB, Raina A, Sethi SS, et al. Impact of interventricular interaction on ventricular function: insights from right ventricular pressure-volume analysis. JACC Heart Fail 2024;12:1179–92.
[34] Arora S, Sivaraj K, Hendrickson M, Chang PP, Weickert T, Qamar A, et al. Prevalence and prognostic significance of mitral regurgitation in acute decompensated heart failure: the ARIC study. JACC Heart Fail 2021;9:179–89.
[35] Cocianni D, Stolfo D, Perotto M, Contessi S, Barbisan D, Savonitto G, et al. Association of tricuspid regurgitation with outcome in acute heart failure. Circ Cardiovasc Imaging 2023;16:566–76.
[36] Butala B, Yu R, Schorr R, Gologorsky E. Periprocedural dynamics of aortic regurgitation in patients supported with an Impella left ventricular assist device. J Cardiothorac Vasc Anesth 2020;34:659–62.
[37] Hiraoka A, Saku K, Nishikawa T, Sunagawa K. A case report of unexpected right-to-left shunt under mechanical support for post-infarction ventricular septal defect: evaluation with haemodynamic simulator. Eur Heart J Case Rep 2021;5:ytab209.